Geostatistical Analysis of Groundwater Levels at Tangab Dam Using IDW, Kriging, and Sequential Gaussian Simulation

Reza Dehshibi[1], Hadi Farhadian[*,2]

1. Department of Engineering, University of Sistan & Baluchestan, Zahedan, Iran.
2. Department of Mining Engineering, Faculty of Engineering, University of Birjand, Birjand, Iran.

***Corresponding Author:**
Hadi Farhadian,

Email: farhadian@birjand.ac.ir
Received: 2025.05.13
Accepted: 2025.07.01
J. Hydraul. Struct., 2025; 12(2):1-21
DOI: 10.22055/jhs.2025.49615.1350

ABSTRACT

Monitoring groundwater levels at every point in dam abutments is often impractical; hence, geostatistical interpolation methods offer a viable alternative. This study applied inverse distance weighting (IDW), kriging, and sequential Gaussian simulation (SGS) to estimate groundwater levels at the Tangab Dam, based on data from 49 piezometers. After data normalization, variogram modeling identified the spherical model as the best fit, with a nugget-to-sill ratio of 19%, indicating strong spatial continuity. While IDW served for initial visualization, kriging and SGS revealed higher groundwater levels along the dam's right abutment, corresponding to fault zones and karst features. The SGS approach, performed through 100 realizations, accurately reproduced the spatial variability and statistical properties of the observed data. Validation showed a correlation coefficient of 0.93 and unbiased residuals, confirming the model's reliability in well-instrumented regions. However, estimations in the northeastern and eastern zones were less reliable due to sparse data. This study underscores the value of integrating geostatistics and geological context for characterizing groundwater behavior in complex karst environments. Future work should involve expanding the monitoring network and coupling geostatistical outputs with numerical flow models to improve prediction and support dam safety assessments.

KEYWORDS
geostatistics, kriging, sequential Gaussian simulation, groundwater level, Tangab Dam.

1. Introduction

One of the fundamental requirements in the exploratory stages of dam construction studies is assessing the permeability and joint conditions, as well as understanding hydrogeochemical behavior [1–3]. Hydrogeological measurements, such as hydraulic conductivity and transmissibility, can exhibit significant uncertainty due to the complexity of geological conditions [4–6]. As a result, various estimation and simulation techniques are employed to address this uncertainty in hydrogeological measurements. In recent years, the uncertainty associated with hydrogeological and geotechnical parameters has been extensively studied, with the hydraulic parameters of the aquifer being estimated using geostatistical methods. The application of geostatistical simulation techniques provides a useful approach to modeling the geometry of permeable layers [7–10].

Previous studies have investigated various aspects of the Tangab Dam site in southern Iran—ranging from karst development and hydraulic connectivity to fault zones and spring origins—each contributing valuable insights yet leaving several research gaps. Akhondi and Mohammadi [11] used 953 water pressure tests to assess the effective porosity and karst development in the Tangab Dam region. Using geostatistical techniques, they examined the behavior of the karst aquifer, the function of the epikarst region, the impact of nutrient input in karst aquifers on spring hydrographs, and the relationship between karstification and permeability (from water pressure tests). According to their study, the length of the major karst channel is one of the most influential factors affecting hydrograph and water fluctuation variations.

In a study by Madani Esfahani and Asghari [12], sequential Gaussian simulation (SGS) was employed to identify areas with varying rock-quality designation (RQD). They found that locations with an RQD of less than 20% were classified as fault areas, while regions with an RQD greater than 50% were less fragmented.

Karimi et al. [13] utilized hydrochemical time series data from springs in the Tangab Dam area to identify the sources of the springs and their interrelationships. The dam site is located between two impassable marl formations and consists of karst limestone and dolomite. The aquifer in the region is drained by 23 springs located to the south. The study measured the main ions, electrical conductivity, temperature, and pH of the springs over a period of 17 months, and they found that four springs were most likely sourced from the southern portion of the region, while the remaining springs were located in both the southern and northern areas.

In another study, Mozafari et al. [14] examined leakage on the right side of the Tangab Dam using a numerical model with SEEP/W software. Their research indicated that the majority of seepage occurred in karst areas, as well as in cracks and crevices.

Asadi [15] employed color detectors to propose two broad models: one for the branching of the main flow transfer channel and the other for identifying the origin of springs in the potential water escape range of the Tangab Dam. The study involved sampling, measuring, and analysis over seven months at 45 locations, with approximately 2000 water samples and 180 bags of activated charcoal evaluated. Their findings underscored the hydrogeological connection between the Tangab region springs and the dam, suggesting that this relationship is facilitated by a single-channel karst system.

Despite these contributions, a critical gap persists in quantitatively characterizing the spatial uncertainty of groundwater level variations—particularly in highly fractured and karstified environments like Tangab—using integrated geostatistical approaches that incorporate both hydrogeological and structural geological data. Huysmans and Dassargues [16] were among the first to apply multiple-point geostatistics in groundwater studies, using an aquifer in Belgium. Their study demonstrated how multiple-point geostatistics could be employed to assess the effects of geological heterogeneity on groundwater flow within the aquifer. They found that pollution clouds resulting from variogram-based simulations expanded more in both the horizontal and vertical directions compared to those simulated with multiple-point geostatistics.

Marache et al. [17] drew a directional variogram along boreholes in a French city. In their study, they used sequential indicator simulation to create a 3D model of geotechnical borehole data (bulk modulus) based on a set of threshold limitations. The results showed that integrating petrological data with geotechnical borehole data improved the simulation outcomes.

Geostatistical methods have been widely used to estimate hydraulic parameters of aquifers and investigate the uncertainty of

hydrogeological and geotechnical parameters. One method for modeling the geometry of permeable layers is geostatistical simulation. This method has been applied in fracture system modeling to study fluid flows inside rocks [18]. The geostatistical simulation method allows for the simulation of variables using statistical parameters derived from spatial data analysis. Sequential indicator simulation, in particular, is one of the most effective approaches for studying the uncertainty of random variables [19].

Furthermore, although studies by Hosseini et al. [20] and Bai et al. [21] highlight the effectiveness of such models in oil fields and groundwater pollution assessment, they do not address spatial uncertainty in groundwater levels in the context of dam safety. The leakage analysis at Tangab Dam, which accounts for both diffuse and conduit flow systems, further underscores the need for spatially explicit models. Under a diffuse flow assumption, leakage remains within acceptable thresholds, but under conduit flow conditions, small-diameter conduits can cause disproportionately high leakage—introducing major uncertainty into design and risk assessments. This necessitates a more rigorous spatial understanding of flow paths and the role of structural geology in controlling permeability, especially in regions outside the proposed grout curtain [22].

In response to these gaps, the primary aim of this study is to investigate groundwater level variations at the Tangab Dam site using an integrated geostatistical approach that combines kriging and Sequential Gaussian Simulation (SGS) with geological fault analysis. Unlike traditional deterministic methods such as IDW, which was applied here solely for preliminary visualization, this study emphasizes the use of SGS through 100 realizations to capture spatial variability and uncertainty in a complex karst aquifer system. By incorporating both hydrogeological data and structural geological features (e.g., fault density), the research provides a more comprehensive model of groundwater behavior. This approach enhances both the reliability of predictions and the interpretability of results, particularly in data-sparse regions. Ultimately, the findings aim to support more informed groundwater management and dam safety strategies in heterogeneous and fractured formations like those at Tangab.

2. Methodology

2.1. Geostatistical Analysis

In classical statistical studies, samples obtained from a population are typically considered random. The measured values of a particular quantity in one sample do not provide any information about the value of the same quantity in another sample. However, in geostatistics, it is possible to establish a relationship between the values of a quantity in the sample population and the distance and orientation of the samples relative to each other. In classical statistics, variability is assumed to be a random variable, whereas in geostatistics, part of this variability is random, and the other part is structured, depending on distance and direction [23].

Therefore, in geostatistics, the presence or absence of spatial structure in the data is first examined. If a spatial structure exists, the data is then analyzed [19]. In geostatistics, adjacent samples may exhibit spatial correlation up to a certain distance. In this case, the probability of similarity between values in closer samples is higher, as spatial structure implies that changes in a given area are more likely to affect nearby areas than those farther away [24,25].

Geostatistics is a branch of statistics based on the theory of regional variables. A regional variable is any variable that is distributed in three-dimensional space and exhibits spatial dependence. Such variables can be investigated in geostatistical studies. For example, the values of the permeability coefficient in a 9×9 km network are considered regional variables. The value of a regional variable Z(x) at any point (Eq. 1) can be decomposed into two components:

deterministic and random. This decomposition is expressed as follows [19]:

$$Z(x) = m(x) + L(x) \quad (1)$$

where Z(x) is the regional variable at coordinates x, L(x) is its random component, and m(x) is its deterministic component.

If a regional variable has an appropriate spatial structure, several analyses can be performed on it, including estimation of the target variable at unsampled locations, sample design, and error variance distribution. Geostatistical estimation begins by identifying and modeling the spatial structure of the variable, which is then, assessed using variogram analysis. The second stage is Kriging estimation. Geostatistical techniques can only be applied if the variable is stationary, which can be verified using a variogram. In linear geostatistics, the data distribution should also approximate a normal distribution [26,27].

2.2. Sequential Gaussian Simulation

Sequential Gaussian Simulation (SGS) is based on the multi-Gaussian model of random functions. Initially, this method was used to simulate a single variable using primary data only; it was later extended to incorporate secondary data and joint modeling approaches. To reproduce the spatial continuity of a variable z at N nodes within a network, the dataset $\{(u_a), a = 1, \dots, n\}$ is utilized. The steps involved in SGS are as follows [28]:

1. Model validation: The validity of the multi-Gaussian random function (RF) model is first assessed. For this, the primary data must be histogrammed, normalized, and transformed from the original z-values to Gaussian y-values using a common cumulative distribution function (CDF).

2. Simulation sequence (if the RF model for y is valid):

- Create a variogram using the normalized data.
- Define a random simulation path such that each node is visited only once.
- At each node, estimate the local mean and variance of the Gaussian CDF using kriging with the variogram model of the normalized data.
- Draw a value from the local CDF and add it to the conditioning dataset.
- Repeat the estimation and simulation steps for each subsequent node along the random path.
- Continue this process until all N nodes in the domain have been simulated.

SGS is computationally efficient because it requires solving only one kriging system per node. However, it has limitations: it may not accurately reproduce extreme (tail) values and can struggle with capturing spatial coherence across distinct value classes. To address these limitations, alternative non-Gaussian simulation algorithms—capable of preserving the continuity of extreme values over short ranges—can be used for improved performance [29].

3. Tangab Dam

3.1. Location and Geology

The Tangab Dam is situated on the Firouzabad River in Fars Province, approximately 90 kilometers south of Shiraz. The dam is located on the Podenow Anticline within the folded zone of the Zagros Mountains (Sadeh Zagros). As reported by Akhondi and Mohammadi [11], the dominant geological unit at the site is the Asmari Limestone Formation (AF), which overlies the Pabdeh-Gurpi Formation (PGF) and is itself overlain by the Razak Formation. To monitor the reservoir and assess subsurface conditions, 49 observation

wells were installed across the left and right abutments of the dam (Figure 1).

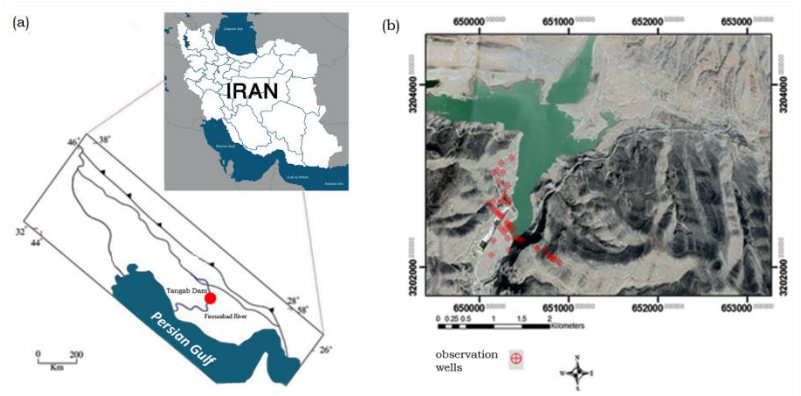


Figure 1. (a) Location of the research area; (b) Location of observation wells in the dam abutment.

The fold structure is predominantly composed of the PGF, AF, and Razak formations. The Firouzabad River has incised a 100-meter-deep channel through the saddle-shaped center of the Podenow Anticline in the Tangab Valley [30]. Prior to dam construction, several springs, with a combined average discharge of approximately 1 m^3/s, were actively discharging from the southern limb of the anticline (Figure 2a). Dye tracing experiments using Rhodamine and Uranine—conducted at the eastern and western abutments of the reservoir—revealed strong hydraulic connectivity within the karst system. The dyes were detected at Tangab and Atashkadeh Springs only a few days after injection [15,30], and the measured tracer velocities confirmed the existence of conduit flow between the northern and southern limbs of the anticline. These findings indicate a significant subsurface water transfer system that bypasses surface constraints. The leakage issue at the site has been extensively investigated by Mozafari et al. [14]. Initially, the site's water-tightness system included a concrete cut-off wall at the dam foundation, accompanied by a single-row grout curtain extending 256 meters into the western abutment and 206 meters into the eastern abutment (Figure 2b). These curtains, penetrating to depths of 80–180 meters, terminated within the AF and lacked connection to adjacent impermeable formations [31].

During the reservoir's first impoundment in 2009, the water level rose to 1413.65 meters above sea level (ASL), which was approximately 34.35 meters below the Normal Water Level Reservoir (NWLR), before dropping to 1405 m ASL over a 74-day period. During this time, whirlpool vortices were observed near the west abutment, and the discharge from the Atashkadeh Springs increased to 2 m^3/s—clear indications of significant leakage. To mitigate the leakage, a 300-meter extension of the grout curtain was added beyond the eastern abutment. Additionally, a new 570-meter grout curtain was constructed along the west side of the valley (Figure 2b). Despite these interventions, leakage rates remained largely unchanged. The reservoir rests against the northern limb of the anticline, in direct contact with the karstified Asmari Limestone Formation and the Razak aquitard. At both abutments, a preferential leakage pathway (PLP) appears to extend from the reservoir to the southern limb of the anticline. The lengths of the inlet windows at NWLR are at least 850 meters on the west and 600 meters on the east. Water is thought to be transmitted through the AF towards potential discharge zones on both riverbanks downstream of the dam. Notably, the PGF lies too deep beneath the central part of the anticline to act as an effective barrier. Ultimately, the initial grout curtains failed to seal the PLP

effectively. Iso-potential mapping revealed that leakage bypassed the ends of the grout curtains and traveled through the preferential pathways, affirming the necessity of further mitigation strategies [14].

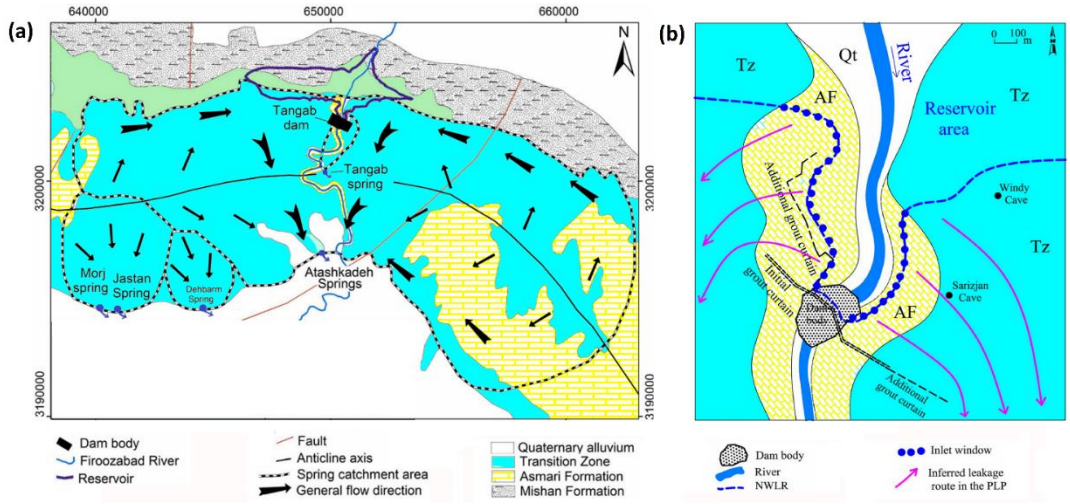


Figure 2. Geological map of (a) the central section of the Podenow Anticline [13] and (b) the Tangab Dam site [14].

3.2. Potential leakage routes

The Tangab Dam is located approximately 1000 meters within the Tangab Valley, where the reservoir water is in direct contact with the Asmari Formation, the Transition Zone, and the Razak Formation, all overlain by alluvial deposits. The Razak Formation and the Transition Zone contain frequent marlstone layers that inhibit vertical water movement, confining leakage pathways primarily to the karstified Asmari Aquifer. Reservoir seepage can occur in two main ways: directly through the Asmari Formation along the valley flanks, or indirectly via the alluvium at the valley floor. However, seepage through the alluvium appears negligible due to:

(a) the absence of vortex features on the reservoir surface, (b) lack of subsidence at the dam body and reservoir bed, and (c) stable readings from piezometers SP1–SP9 and FO-PIZ1 downstream of the cut-off wall and grout curtain (Figure 3).

At the left abutment, neither the original nor extended grout curtains intersect the key leakage window, as they are oriented nearly perpendicular rather than parallel to the valley slope (Figure 3). Although these curtains were designed to seal into the dense dolomitic limestone, water movement persists within this layer, especially in high-permeability zones (up to 100 Lu) with substantial grout take (>400 kg/m). Piezometers LG1P4U to LG1P14U (upstream) and LG1P1D to LG1P13D (downstream) installed in Gallery LG1 monitor hydraulic behavior around the grout curtains. On the right abutment, the initial grout curtain was similarly oriented perpendicular to the valley side, while subsequent curtains were aligned more parallel to the valley. However, these measures failed to fully seal the reservoir due to incomplete contact with the underlying Pabdeh Formation and lateral boundaries with the Razak Formation. As a result, water continues to bypass the grout curtains downstream. Piezometers RG2P1–RG2P7C in Gallery RG2 (downstream) and RBP1–RBP16 monitor leakage around both the initial and additional grout curtains. Geomorphologically, the Firouzabad River appears to be superimposed on the central part of the Podenow Anticline, where it incised the valley and likely established pathways for karst development. Portions of the riverbed on the northern limb are at higher elevations, allowing water

infiltration into the karst aquifer on the southern limb, particularly along faulted zones. Over geological time, these pathways evolved into mature conduits. The general alignment of the Windy and Sarizjan caves toward the southern limb supports this interpretation, suggesting paleo-flow from north to south. As the river downcut, older conduits became inactive, leaving abandoned cave levels now exposed at higher elevations. This proposed leakage route is further supported by two dye-tracing experiments conducted prior to dam construction. Although this pathway would require cross-bedding flow, the F1 and F2 faults—both striking roughly perpendicular to the fold axis—intersect bedding planes and likely facilitate such movement. At the left abutment, the F1 Fault aligns with the Tangab Spring. However, no significant increase in spring discharge was observed post-impoundment, likely due to extensive grouting in this area (Zone A, Figure 6). On the right abutment, water likely enters the karst system through the F4, F6, and F7 faults, further contributing to downstream leakage (Figure 3) [14,31].

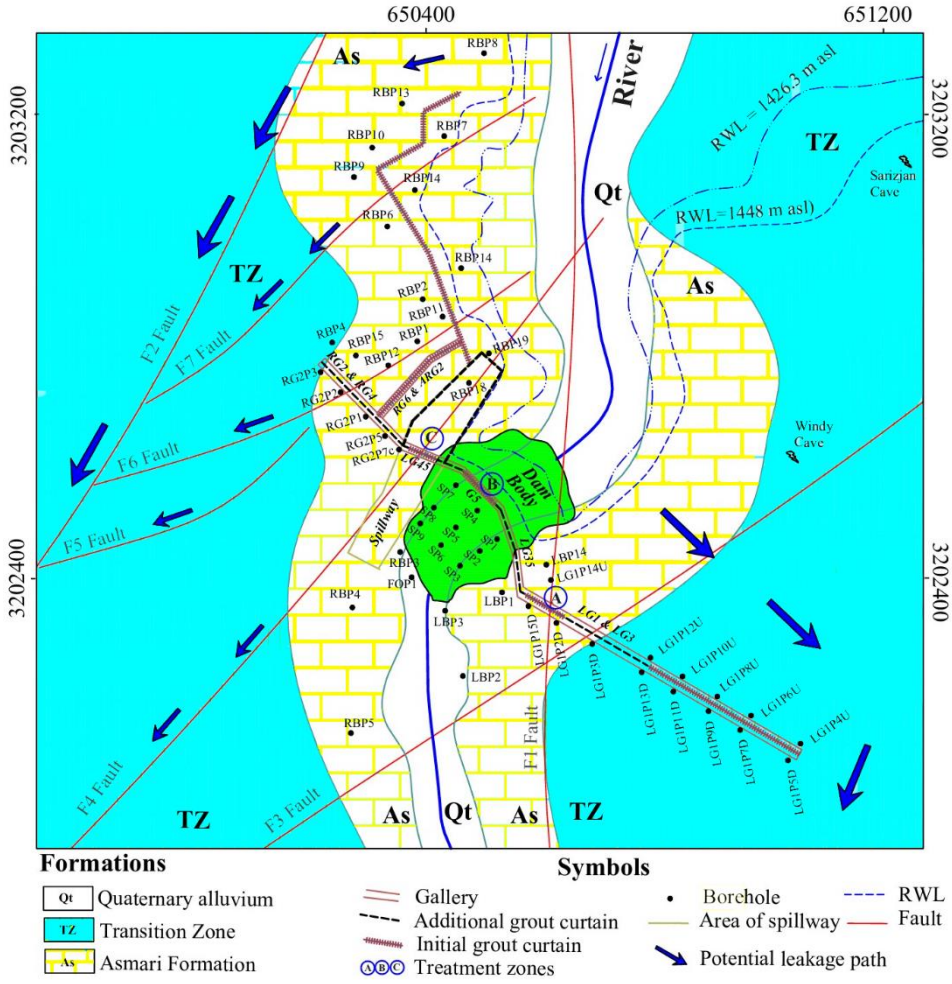


Figure 3. Engineering overlay on the geological map of the Tangab Dam site [14]

4. Discussion and results

4.1. Investigation of Groundwater Level Using the Sequential Gaussian Simulation Method

Initially, the distance-weighted interpolation method was applied using ArcMap to gain a preliminary understanding of spatial variations across the study area. This method, often referred to as the "photo distance" approach, provides estimated values that closely

resemble the observed data but does not support the generation of uncertainty maps. It is primarily used for initial visualization and pattern recognition.

Following this, the dataset was normalized, and spatial continuity was assessed by constructing a variogram. Geostatistical interpolation was then conducted using the kriging method, which also facilitated the creation of an uncertainty map. Finally, based on the kriging estimates, 100 sequential Gaussian simulations were performed in the study area using ISATIS software. The outputs of these simulations provide a spatially continuous depiction of groundwater levels throughout the dam abutments.

4.2. Exploratory Data Analysis

Table 1 presents the descriptive statistics for groundwater level measurements obtained from 49 piezometers. For effective interpolation and simulation, it is necessary for the data to follow a normal distribution. As shown in Figure 4a, the histogram of the raw water level data indicates non-normality, with a standard deviation of 12.54, skewness of 0.63, and kurtosis (elongation) of 4.02. Therefore, Gaussian normalization was applied. The resulting histogram of the normalized data is presented in Figure 4b, demonstrating improved statistical distribution suitable for geostatistical modeling.

Table 1. Descriptive statistics

Value	Frequency	Min (m)	Max (m)	Average (m)	Standard Deviation	Variance
Water lable	49	1362.99	1424.81	1382.25	12.54	157.25

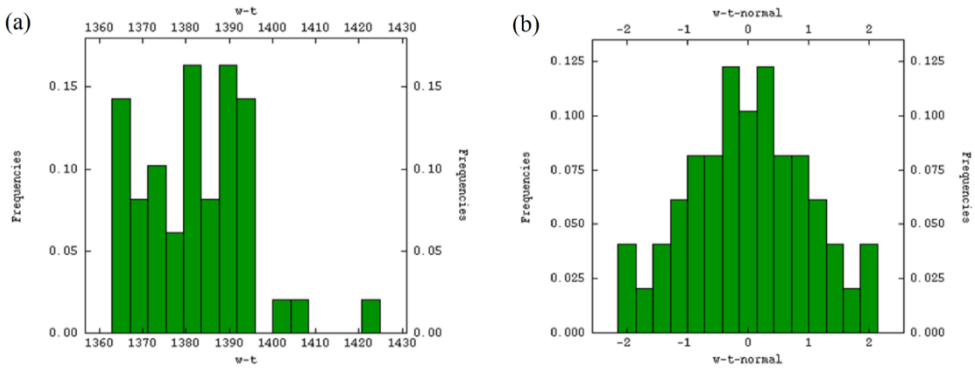


Figure 4. (a) Histogram of original water level data; (b) Histogram after Gaussian normalization.

4.3. Variable Spatial Continuity

Figure 5 presents the experimental variogram of groundwater levels along with the fitted spherical model. The spatial continuity of the water level was assessed through this variogram analysis. The degree of spatial structure is quantified using the nugget-to-sill ratio (referred to here as the "piece effect to roof ratio"). According to Isaaks and Srivastava [19], a ratio of less than 25% indicates strong spatial dependence, a ratio between 25% and 75% reflects moderate spatial dependence, and a ratio greater than 75% suggests weak spatial dependence. In this study, the spherical model showed a ratio within the range that implies a reasonable level of spatial correlation, thereby justifying the use of geostatistical interpolation methods such as kriging.

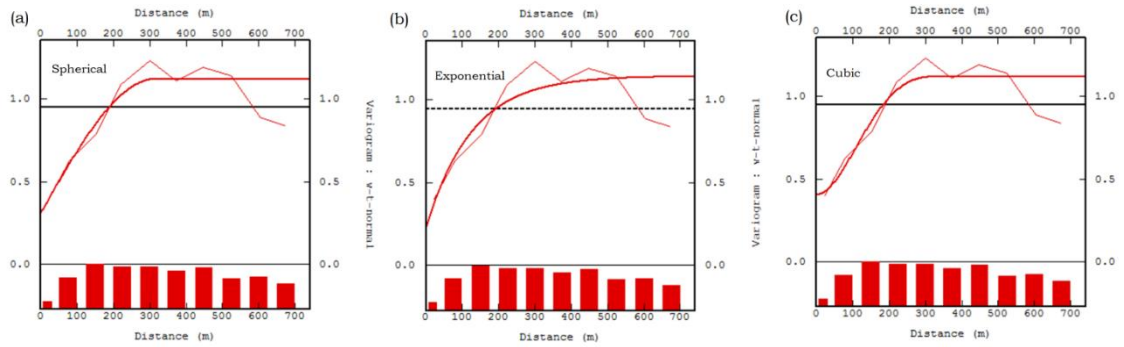


Figure 5. Experimental variograms of water level with fitted models: (a) spherical; (b) exponential; (c) cubic.

In this study, the exponential, spherical, and cubic variogram models exhibited nugget-to-sill ratios of 19%, 27%, and 35%, respectively. These values indicate that the exponential model demonstrates strong spatial continuity, while the spherical and cubic models exhibit moderate spatial dependence. Additionally, a larger range (or radius of influence) reflects a broader spatial structure, meaning fewer sampling points are needed to predict unsampled values with confidence. The range values for the exponential, spherical, and cubic models were 416.38 meters, 322.86 meters, and 376.6 meters, respectively. Among the three, the spherical model yielded the lowest sum of squared residuals, as shown in Table 2, indicating the best fit for subsequent kriging and simulation procedures.

Table 2. Variogram Features with a suitable spherical model

Model	Exponential	Spherical	Cubic
Nugget effect	0.23	0.31	0.41
Domain	416.38m	322.86	376.6
Threshold	0.95	0.82	0.73
Sum of squared residuals	0.000877	0.000527	0.000585
c_0+c	1.18	1.13	1.14
c_0/c	0.194915254	0.274336283	0.359649123

4.4. Variogram Validation

Several variogram models with different structural characteristics were considered to simulate the experimental variogram. Choosing an appropriate model and accurately estimating its parameters is critical, as these directly affect the reliability of geostatistical estimations. In this study, a cross-validation procedure was used to assess the accuracy and appropriateness of the selected variogram model. During cross-validation, one data point is removed at a time, and its value is estimated using the remaining dataset via the kriging method. This process is repeated sequentially for all data points. The differences between observed and estimated values were used to generate a correlation map, evaluating how well the model reproduces the actual data. Using the validation function in ISATIS software, a correlation coefficient of 0.73 was obtained between the observed and estimated groundwater levels, indicating a good level of agreement. Furthermore, the residual distribution (actual minus estimated values)

was plotted to assess the bias of the model. As shown in Figure 6, the residuals are symmetrically distributed around zero, confirming that the model is unbiased. Additionally, the normal probability plot in Figure 7 demonstrates that the residuals approximate a normal distribution, further validating the suitability of the selected variogram.

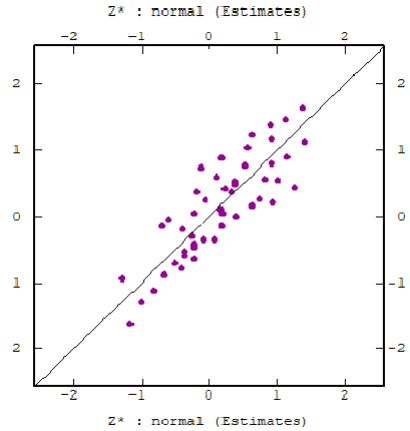


Figure 6. Cross-validation error distribution (residuals) between observed and kriging-estimated water levels.

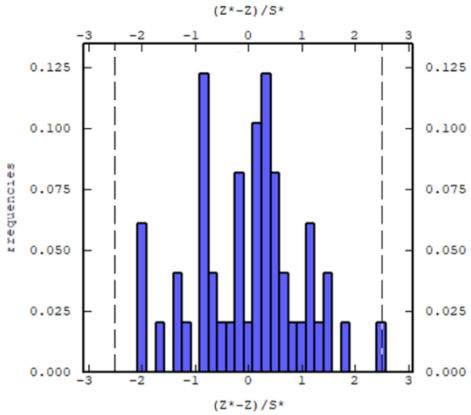


Figure 7. Normal probability plot of residuals from variogram cross-validation

4.5. Water Level Interpolation Using the IDW Method

The Inverse Distance Weighting (IDW) interpolation method has been employed as one of the precise and effective techniques for understanding and gaining a broad perspective of the spatial variations in water levels within the examined area. In this method, the estimated values closely resemble the observed sampling values. However, the estimated values may diverge from the sampled values in cases of imprecise data. Unlike some other methods, the distribution of data surrounding the estimated point is not directly taken into account. Instead, the position of each point is considered individually, with the weights assigned to points that are equidistant from the target point. The deterministic nature of the IDW method does not produce an uncertainty map and does not make assumptions about the data, such as the normality requirement that is typically necessary for geostatistical methods. The appropriate values for the power parameter, the number of neighboring points, and the search radius have been determined in this approach (Table 3). The interpolated map resulting from the IDW method is shown in Figure 8.

Table 3. Parameters to calculate IDW interpolation

Method	Inverse Distance Weighted Interpolation
Power	2
Max-Neighbors	10
Min-Neighbors	5
Major semiaxis	100
Minor semiaxis	100

The observed and estimated water levels of the observation wells are derived from the interpolation of the water levels, and the difference between these two values is indicated as the error in Figure 9. The distribution of the estimated and observed values, along with the best-fit line between them, determines the shape of the state diagram. The accuracy of the model's estimation increases as the values approach the 1:1 line. The regression equation was used to estimate the points, and the interpolation error is approximately 0.2. The independence of errors is a key assumption in regression analysis. If the errors are correlated, regression cannot be applied.

The Durbin-Watson test is used to assess the independence of errors. Based on the results shown in Figure 9, the error value is 1.85, indicating that the results are reliable, as the Durbin-Watson statistic (DW) lies between 1.5 and 2.5. If DW falls outside of this range, it confirms the presence of autocorrelation in the errors.

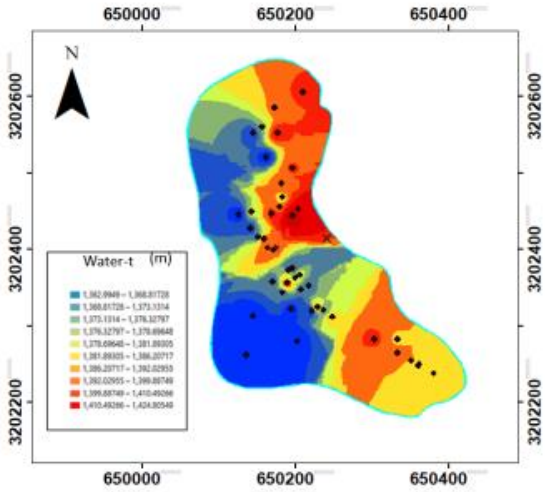


Figure 8. Water level interpolation using the IDW method.

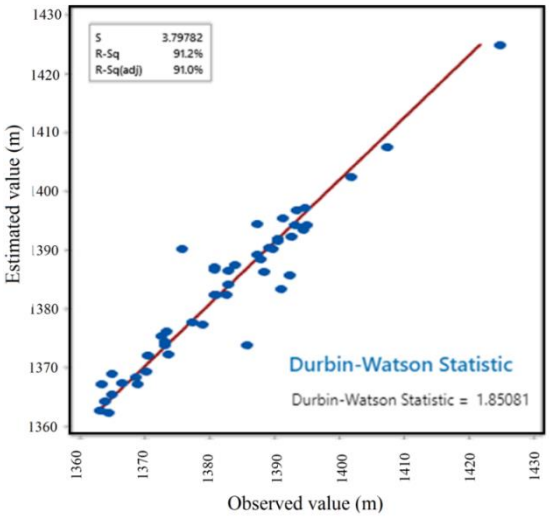


Figure 9. Correlation between the estimated and observed values of the water level in the IDW method, as assessed by the Durbin-Watson test.

4.6. Interpolation Using the Kriging Method

The water levels at unknown sites around the dam have been estimated using the normal data of the reservoir level and the exponential variogram model. The reservoir level was then interpolated (Figure 10a). As shown in the uncertainty map and the interpolation error value in Figure 10b, the estimation error is higher in areas with fewer data points or no water level measurements. Specifically, the estimations in the northern and eastern regions of the study area are considered unreliable.

Kriging-based techniques, such as sequential conditional simulation methods, analyze sampling points sequentially and randomly until all sampled points have been assessed. One of the key outcomes of using geostatistical methods is identifying the uncertainty surrounding the estimations. The error variance in the standard geostatistical approach is used to quantify this uncertainty. If the assumption of a Gaussian distribution holds, the estimate and error variance together fully represent the uncertainty at each unsampled location. While error variance can accurately predict the arrangement and location of nearby samples, it cannot precisely capture local uncertainty. Specifically, it overlooks regional uncertainty caused by spatial variations within the target area.

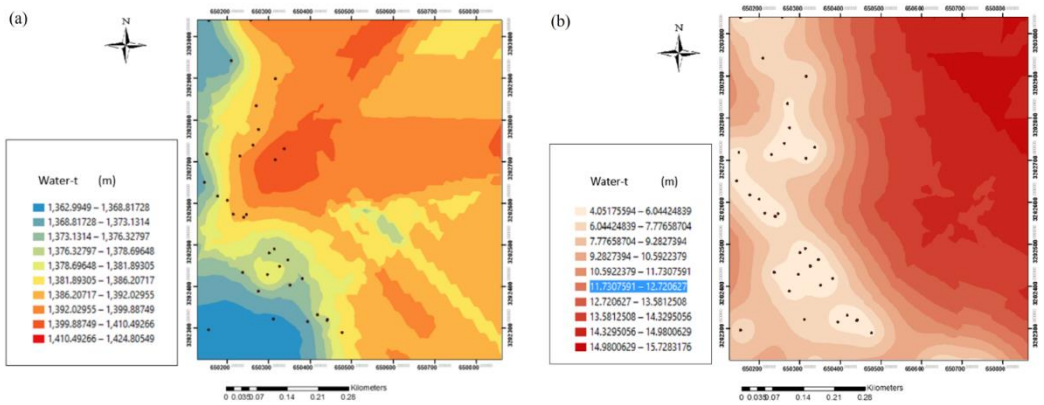


Figure 10. (a) Water level interpolation using Kriging method; (b) Error and uncertainty map resulting from kriging interpolation method.

Alternate probability images are generated through conditional simulation to account for local variability. Estimates and their associated uncertainties are defined and determined using a range of probabilities, incorporating local variability. In the next step, we perform a Gaussian simulation with 100 realizations and assess the results. The analyzed area has undergone 100 successive Gaussian simulations for the water level variable. Figure 11 illustrates the three-dimensional block of the simulation, with multiple layers of the simulation's output visible. Given the breadth of results, it is advisable to compute the average result of the simulation, which is discussed in the next phase, to determine the water level at a specific location.

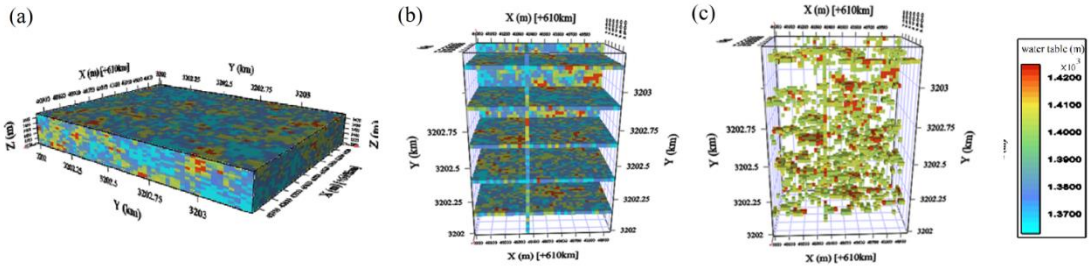


Figure 11. (a) 3D block model of SGS results; (b) Representative layers from simulations; (c) Zones with higher groundwater levels.

4.7. Mathematical Expectation of the Simulation

The average of the 100 realizations from the Gaussian simulation performed in the previous stage should be calculated, considering the comprehensiveness of the data and identifying the regions where water table changes are most pronounced (Figure 12). The estimated average value, visible at various levels in the figure, is consistent with the estimate generated using the kriging method.

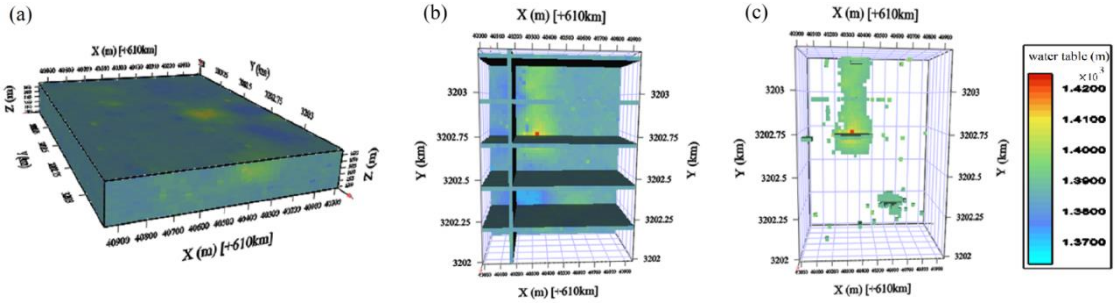


Figure 12. (a) average results of Gaussian simulation block in three dimensions; (b) average results of Gaussian simulation in different levels; (c) display of higher water level values in levels

At this stage, the exploratory analysis for each level is presented in Table 4, based on simulations run along the z-axis at 150 meters (15 cells, each 10 meters) in the direction of the boreholes. In the diagram, height is plotted against the range of changes for each level, with the range of extreme changes for some levels indicating larger values relative to smaller ones, which have a higher level of stability. The graph shows that as the height level increases, the variations in water level also increase.

In a karst system, two piezometers may be close to one another but not connected. On the other hand, the non-uniform depth of observation wells is the most significant issue in our analysis. While there is no guarantee in a karst system, this issue is

presented as a possibility: as the depth of an observation well increases, it is possible that a new layer of permeable material is encountered, which could cause the water level to either rise or fall.

To conduct a more detailed investigation and precisely identify locations where the water level is higher or lower than the average, it is preferable to display a map for each level separately, with a distance of 10 meters between each point. The maps obtained at various levels are shown in Figure 13.

Table 4. Descriptive statistics of different levels

number	from	to	Minimum	Maximum	Mean	Std.	Variance
1	1350	1360	1368.2	1394.82	1383.26	2.46	6.03
2	1360	1370	1368.3	1396.21	1383.14	2.58	6.66
3	1370	1380	1362.99	1404.34	1383.08	2.86	0.82
4	1380	1390	1367.98	1393.57	1382.9	3.18	10.09
5	1390	1400	1367.39	1400.33	1382.78	3.55	12.59
6	1400	1410	1364.37	1402.95	1382.75	3.77	14.22
7	1410	1420	1362.99	1397.63	1382.89	4.08	16.61
8	1420	1430	1362.99	1398.57	1383.13	4.35	18.89
9	1430	1440	1366.95	1406.13	1383.24	4.53	20.52
10	1440	1450	1368.26	1411.93	1383.5	4.79	22.91
11	1450	1460	1362.99	1410.06	1383.77	4.91	24.11
12	1460	1470	1363.28	1412.65	1383.95	4.73	22.35
13	1470	1480	1370.2	1424.59	1384.1	0.46	2.12
14	1480	1490	1369.09	1424.81	1384.1	4.36	18.99
15	1490	1500	1372.14	1413.21	1384.2	4.16	17.35

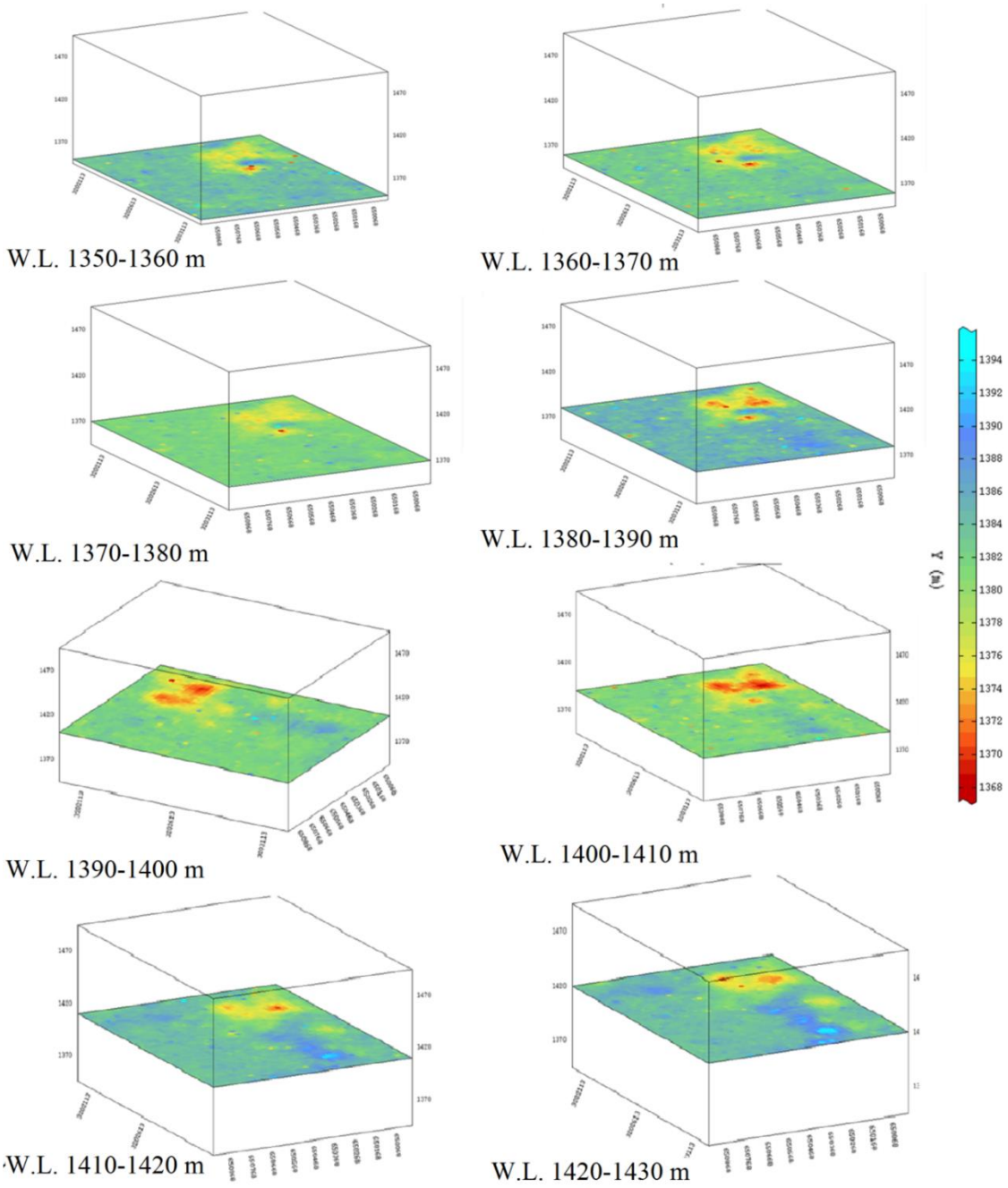


Figure 13. Simulated groundwater levels at 15 depth intervals (10 m each) from 1350 to 1430 m elevation.

The next step is to create a plan map, which represents the average of the various levels of the simulated block, for a more in-depth analysis. The output of the simulated average can be viewed in the two-dimensional map after the three-dimensional network, where 100 realizations of the simulation were conducted, has been transformed into a two-dimensional network. As shown in Figure 14a, reveals a clear groundwater mound in the north-central area, which may be attributed to topographic influences, recharge zones, or structural features (e.g., faults/fractures) facilitating upward flow. Also, Figure 14b overlays the same data on

the topographic landscape. Elevated groundwater zones appear to align with surface highs, suggesting a good correlation between topography and water table elevation. This might also reflect subsurface geological controls (e.g., permeable formations or fractures). The proximity of high groundwater levels to the reservoir indicates a potential hydraulic connection that may pose seepage or uplift risks for dam stability.

Additionally, the fault map in Figure 15 suggests that the density of faults in this region may contribute to the high water level variations on the right side of the dam. The F3 fault is of particular concern due to its orientation crossing beneath or adjacent to the reservoir. This suggests it may serve as a preferential path for groundwater movement or even seepage under pressure. The intersection of multiple faults in this region increases the potential for fracture permeability, which could amplify hydraulic connectivity and challenge dam safety or groundwater modeling accuracy. These structural features should be further evaluated for their hydrogeological behavior, especially in scenarios involving reservoir level fluctuations or seismic activity.

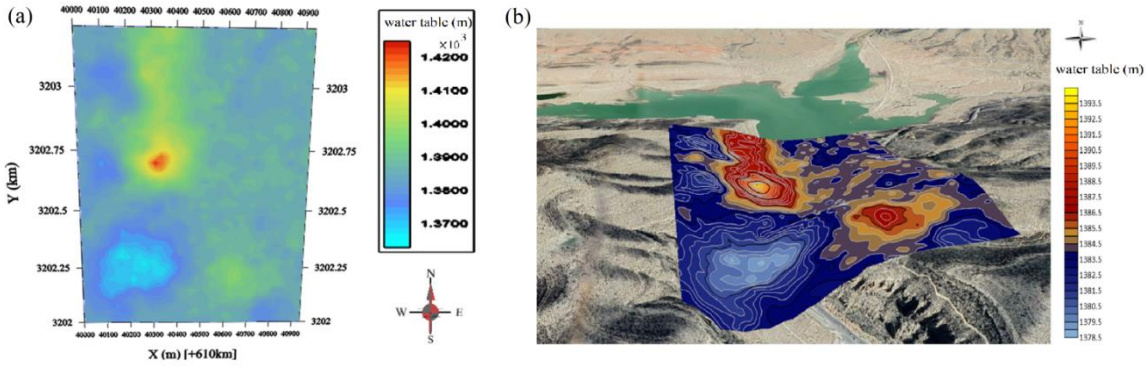


Figure 14. (a) Groundwater table distribution from Gaussian simulation showing high and low zones; (b) 3D view of the water table over terrain, highlighting elevated groundwater areas near the dam reservoir.

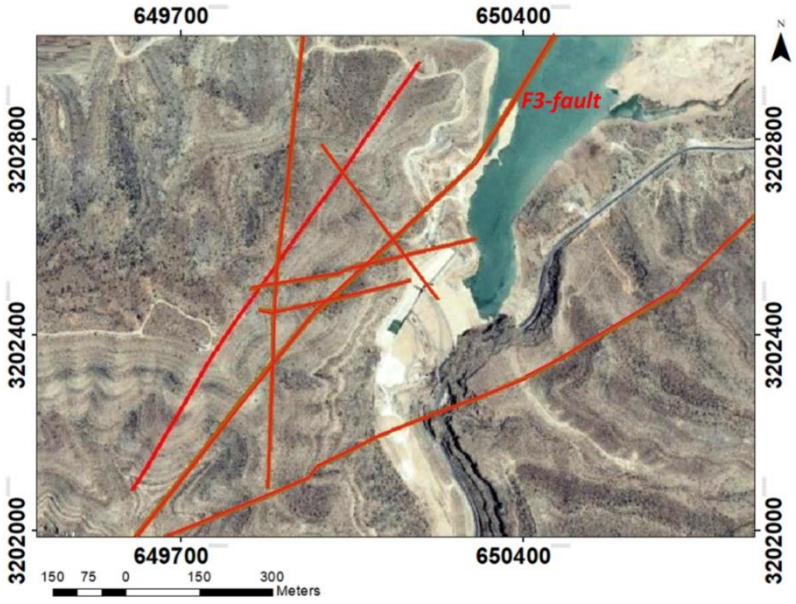


Figure 15. Fault density map on the dam's right abutment

4.8. Validation of Simulation Results

The simulation results (realizations) are considered acceptable when they can reproduce the statistical and geostatistical parameters of the exploration data. Figure 16 shows the histogram of the actual data (exploratory borehole data) alongside the frequency diagram obtained from the simulation results for this purpose. As observed, the average result of the simulation is nearly identical to the average result from the statistical analysis of the exploratory well data. Therefore, the simulation results accurately reproduce the statistical parameters of the data and are deemed valid.

Based on the average water level data, the variogram's segment-to-ceiling ratio is 19%, indicating that the water table level variable exhibits a fair degree of continuity. The results of the water table estimation revealed that the northeastern and eastern regions of the study area had unreliable water table estimations, which may have been caused by a lack of water table data in those regions.

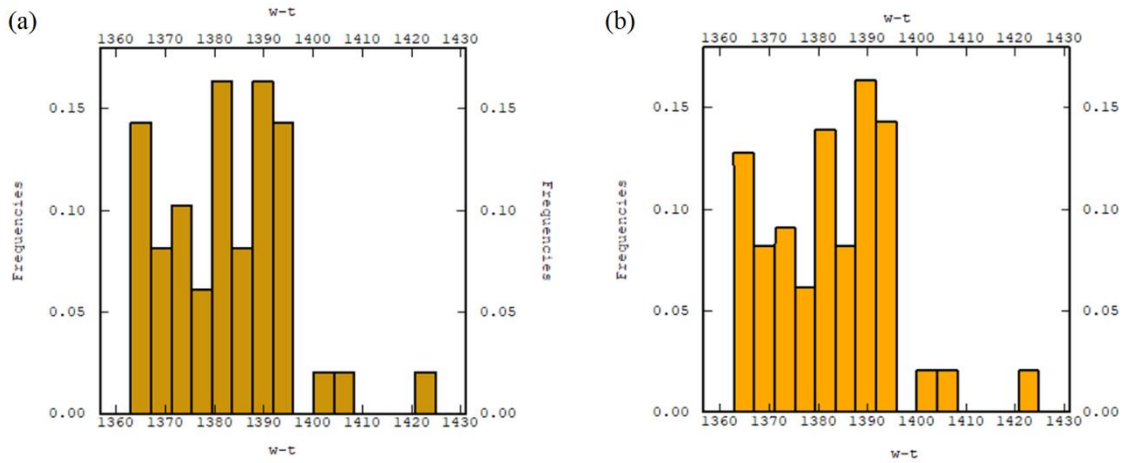


Figure 16. (a) Histogram of the actual data (exploratory borehole data); (b) Frequency diagram obtained from the simulation results.

In summary, the methodological framework of this study follows a structured and sequential approach designed to ensure robust groundwater level modeling in a complex karstic environment. The process begins with exploratory data analysis and normalization to meet the statistical requirements of geostatistical modeling. This is followed by variogram construction and model selection, where the spherical model was identified as the best fit based on the nugget-to-sill ratio and minimal residual error. Kriging is then applied to estimate spatial distributions, while Sequential Gaussian Simulation (SGS) with 100 realizations is used to capture local variability and uncertainty. Finally, the results are interpreted in conjunction with geological structures, particularly fault distributions, to better understand groundwater flow dynamics. This integrated methodology not only enhances the spatial accuracy of predictions but also provides a more realistic representation of uncertainty, making it a valuable tool for hydrogeological analysis and dam safety assessment in heterogeneous terrains.

4.9. Comparison of Interpolation Methods

To evaluate the relative performance of the three applied spatial estimation techniques—Inverse Distance Weighting (IDW), kriging, and Sequential Gaussian Simulation (SGS)—a comparative analysis was conducted based on interpolation accuracy, uncertainty representation, and spatial realism.

IDW was primarily used as a deterministic method for preliminary

visualization. It closely replicates observed data in areas with dense sampling but lacks the ability to model uncertainty or account for spatial correlation. The method assumes a uniform influence radius and is sensitive to outliers.

Kriging, a geostatistical estimator, improved upon IDW by incorporating spatial structure via a fitted variogram model. It provided smoother interpolations and generated an uncertainty map (kriging variance), which is valuable for evaluating prediction confidence. However, as a linear estimator, kriging tends to underestimate variability, especially in heterogeneous regions.

SGS offered a probabilistic modeling approach through 100 realizations, capturing both spatial variability and uncertainty more realistically. It was particularly effective in representing local fluctuations in water level, especially in faulted or karstic zones. SGS outputs also allowed the generation of 3D groundwater distribution models and probability maps, which are critical for risk analysis and decision-making in dam engineering. A summary of the performance characteristics of each method is provided in Table 5.

Table 5. Summary of the performance characteristics of IDW, Kriging, and SGS methods

Method	Type	Strengths	Limitations	Error/Validation Metrics
IDW	Deterministic	Simple, fast, intuitive for initial trends	No uncertainty modeling, sensitive to outliers	DW = 1.85, Error ≈ 0.2
Kriging	Geostatistical	Accounts for spatial continuity, provides variance map	May smooth data, underrepresents extremes	Correlation = 0.93, unbiased residuals
SGS	Stochastic	Captures spatial variability, uncertainty, and extreme values	Computationally intensive, requires variogram model	Closely matched observed mean, strong visual agreement

This comparative evaluation demonstrates that while IDW is suitable for initial analysis, kriging and SGS offer significant improvements for modeling in complex hydrogeological settings. SGS, in particular, emerges as the most robust method for groundwater level estimation in the Tangab Dam's karst terrain due to its ability to quantify uncertainty and replicate natural spatial variability.

5. Conclusion

This study applied a combination of geostatistical techniques—including inverse distance weighting (IDW), kriging, and sequential Gaussian simulation (SGS)—to estimate and analyze groundwater levels at the Tangab Dam using piezometric data from 49 observation wells. Preliminary statistical analysis revealed non-normality in the raw data, necessitating normalization before variogram modeling. Among the tested models, the spherical variogram exhibited the best fit with a nugget-to-sill ratio of 19%, indicating strong spatial continuity and justifying the application of geostatistical methods.

While IDW served as a preliminary visualization tool, kriging and SGS provided more accurate and interpretable insights into spatial trends. Both methods revealed elevated groundwater levels along the dam's right abutment—an area of high fault density—suggesting that geological structures significantly influence groundwater movement. SGS, through 100 realizations, successfully reproduced both the statistical distribution and spatial variability of the aquifer, with a strong match to empirical data. Validation metrics confirmed the robustness of the simulation, especially in well-instrumented regions, while acknowledging limitations in data-sparse zones such as the northeast and east.

Importantly, this study highlights the value of integrating geostatistical modeling

with geological fault data to improve the understanding of groundwater flow in complex karst environments. These findings carry practical implications for dam safety, as zones of elevated groundwater near fault intersections may pose seepage or uplift risks. Based on this, targeted recommendations include reinforcing monitoring systems in critical zones, expanding the piezometer network—especially in under-sampled areas—and using geostatistical uncertainty maps to prioritize grouting and sealing operations.

Future work should focus on enhancing spatial resolution through additional borehole data and incorporating numerical groundwater flow models to better simulate dynamic hydrological conditions. This integrated approach would support more effective groundwater management and risk mitigation strategies in structurally complex dam sites like Tangab.

Fundings
This research received no external funding.

Conflict of Interest
The authors declare that they have no conflict of interest.

Author Contributions
All authors contributed to the study conception and design.

References

1. Farhadian H, Bahmani Shahraki F. Enhancing analytical methods for estimating water inflow to tunnels in the presence of discontinuity areas. Environ Earth Sci. 2024;83:339.
2. Anvari AA, Katibeh H, Sharifzadeh M, Farhadian H. Estimation of fault zone permeability with fuzzy-delphi AHP (FDAHP) method. Rock Mech Civ Environ Eng - Proc Eur Rock Mech Symp EUROCK 2010. 2010. https://doi.org/10.1201/b10550-56
3. Qi S, Wen Z, Lu C, Shu L, Shao J, Huang Y, et al. A new empirical model for estimating the hydraulic conductivity of low permeability media. Proc Int Assoc Hydrol Sci. 2015;368:478–83. https://doi.org/10.5194/piahs-368-478-2015
4. Farhadian H, Nikvar-Hassani A. Water flow into tunnels in discontinuous rock: a short critical review of the analytical solution of the art. Bull Eng Geol Environ. 2019;78:3833–49. https://doi.org/10.1007/s10064-018-1348-9
5. Farhadian H, Maleki Z, Eslaminezhad SA. Assessment of the Optimum Depth of Sealing Cutoff Walls in the Clay Core of Peygham-Chay Dam. J Hydraul Struct. 2021;7:59–76. https://doi.org/10.22055/jhs.2021.37119.1168
6. Nikvar Hassani A, Farhadian H, Katibeh H. A comparative study on evaluation of steady-state groundwater inflow into a circular shallow tunnel. Tunn Undergr Sp Technol. 2018;73. https://doi.org/10.1016/j.tust.2017.11.019
7. Dehshibi R, Karami S, Maleki Z, Farhadian H. A comparative study on evaluation of steady-state groundwater quality in Sirjan's Golgohar mineral zone. Arab J Geosci. 2022;15:1–20. https://doi.org/10.1007/s12517-022-10074-w
8. Goovaerts P. Geostatistical approaches for incorporating elevation into the spatial interpolation of rainfall. J Hydrol. 2000;228:113–29. https://doi.org/10.1016/S0022-1694(00)00144-X
9. Barca E, Passarella G. Spatial evaluation of the risk of groundwater quality degradation. A comparison between disjunctive kriging and geostatistical simulation. Environ Monit Assess. 2008;137:261–73. https://doi.org/10.1007/s10661-007-9758-3
10. Rajaee T, Nourani V, Pouraslan F. Groundwater level forecasting using wavelet and kriging. J Hydraul Struct. 2016;2:1–21. https://jhs.scu.ac.ir/article_12848.html
11. Akhondi M, Mohammadi Z. Preliminary analysis of spatial development of karst using a geostatistical simulation approach. Bull Eng Geol Environ. 2014;73:1037–47. https://doi.org/10.1007/s10064-014-0599-3
12. Madani Esfahani N, Asghari O. Fault detection in 3D by sequential Gaussian

simulation of Rock Quality Designation (RQD) Case study: Gazestan phosphate ore deposit, Central Iran. Arab J Geosci. 2013;6:3737–47. https://doi.org/10.1007/s12517-012-0633-3
13. Karimi H, Raeisi E, Zare M. Physicochemical time series of karst springs as a tool to differentiate the source of spring water. Carbonates and Evaporites. 2005;20:138–47. https://doi.org/10.1007/BF03175457
14. Mozafari M, Milanović P, Jamei J. Water leakage problems at the Tangab Dam Reservoir (SW Iran), case study of the complexities of dams on karst. Bull Eng Geol Environ. 2021;80:7989–8007. https://doi.org/10.1007/s10064-021-02387-z
15. Asadi N. The study of water tightness problem in Tangab Dam by use of dye tracers [M. Sc. Thesis (in Farsi)]: Dept. of Earth Sciences. Shiraz Univ Shiraz, Iran. 1998;
16. Huysmans M, Dassargues A. Application of multiple-point geostatistics on modelling groundwater flow and transport in a cross-bedded aquifer. Hydrogeol J. 2009;17. https://doi.org/10.1007/s10040-009-0495-2
17. Marache A, Breysse D, Piette C, Thierry P. Geotechnical modeling at the city scale using statistical and geostatistical tools: The Pessac case (France). Eng Geol. 2009;107:67–76. https://doi.org/10.1016/j.enggeo.2009.04.003
18. Jaquet O, Siegel P, Klubertanz G, Benabderrhamane H. Stochastic discrete model of karstic networks. Adv Water Resour. 2004;27:751–60. https://doi.org/10.1016/j.advwatres.2004.03.007
19. Isaaks EH, Srivastava RM. Applied geostatistics. 1989;
20. Hosseini E, Gholami R, Hajivand F. Geostatistical modeling and spatial distribution analysis of porosity and permeability in the Shurijeh-B reservoir of Khangiran gas field in Iran. J Pet Explor Prod Technol. 2019;9:1051–73. https://doi.org/10.1007/s13202-018-0587-4
21. Bai L, Cai J, Liu Y, Chen H, Zhang B, Huang L. Responses of field evapotranspiration to the changes of cropping pattern and groundwater depth in large irrigation district of Yellow River basin. Agric Water Manag. 2017;188:1–11. https://doi.org/10.1016/j.agwat.2017.03.028
22. Farhadian H. A new empirical chart for rockburst analysis in tunnelling: Tunnel rockburst classification (TRC). Int J Min Sci Technol. 2021; https://doi.org/10.1016/j.ijmst.2021.03.010
23. Shademan M, Farhadian H. Contribution of geostatistical modeling on simulating a geomechanical parameter (case study: GSI in Gol-Gohar open pit iron mine, Kerman, southeastern Iran). J Geomine. 2023;1:81–91. 10.22077/jgm.2023.6696.1013
24. Farhadian H, Nikvar-Hassani A. Development of a New Empirical Method to Tunnel Squeezing Classification (TSC). Q J Eng Geol Hydrogeol. 2020; https://doi.org/10.1144/qjegh2019-108
25. Journel AG. Modelling uncertainty and spatial dependence: stochastic imaging. Int J Geogr Inf Syst. 1996;10:517–22. https://doi.org/10.1080/02693799608902094
26. Farhadian H, Maleki Z. Groutability classification of granular soils with cement grouts. J Rock Mech Geotech Eng. 2023;15:1580–90. https://doi.org/10.1016/j.jrmge.2022.09.007
27. Deutsch C V. Geostatistical modelling of geometallurgical variables—Problems and solutions. Proc Int Geometallurgy Conf Brisbane, Aust. 2013.
28. Rossi ME, Deutsch C V, Rossi ME, Deutsch C V. Recoverable Resources: Simulation. Miner Resour Estim. 2014;167–92. https://doi.org/10.1007/978-1-4020-5717-5_10
29. Mohammadi Z, Raeisi E, Bakalowicz M. Method of leakage study at the karst dam site. A case study: Khersan 3 Dam, Iran. Environmental Geology. 2007;52:1053–65.
30. Farhadian H. A new empirical chart for rockburst analysis in tunnelling: Tunnel rockburst classification (TRC). Int J Min Sci Technol. 2021; https://doi.org/10.1016/j.ijmst.2021.03.010
31. Shademan M, Farhadian H. Contribution of geostatistical modeling on simulating a geomechanical parameter (case study: GSI in Gol-Gohar open pit iron mine, Kerman, southeastern Iran). Journal of Geomine. 2023;1:81–91. 10.22077/jgm.2023.6696.1013

32. Farhadian H, Nikvar-Hassani A. Development of a New Empirical Method to Tunnel Squeezing Classification (TSC). Quarterly Journal of Engineering Geology and Hydrogeology. 2020; https://doi.org/10.1144/qjegh2019-108
33. Journel AG. Modelling uncertainty and spatial dependence: stochastic imaging. International Journal of Geographical Information Systems. 1996;10:517–22. https://doi.org/10.1080/02693799608902094
34. Farhadian H, Maleki Z. Groutability classification of granular soils with cement grouts. Journal of Rock Mechanics and Geotechnical Engineering. 2023;15:1580–90. https://doi.org/10.1016/j.jrmge.2022.09.007
35. Deutsch C V. Geostatistical modelling of geometallurgical variables—Problems and solutions. Proceedings of the International Geometallurgy Conference, Brisbane, Australia. 2013.
36. Rossi ME, Deutsch C V, Rossi ME, Deutsch C V. Recoverable Resources: Simulation. Mineral Resource Estimation. 2014;167–92. https://doi.org/10.1007/978-1-4020-5717-5_10
37. Talaei H. Investigation on the flow path through the karstic formation of the left abutment of Tangab Dam by the means of Rhodamine-B dye tracer [M. Sc. Thesis (in Farsi)]: Dept. of Earth Sciences. Shiraz University, Shiraz, Iran. 1999;
38. Mozafari M, Raeisi E. Potential leakage paths at the dams constructed on karst terrains in Iran. Quarterly Journal of Engineering Geology and Hydrogeology. 2022;55:qjegh2021-102.

© 2025 by the authors. Licensee SCU, Ahvaz, Iran. This article is an open access article distributed under the terms and conditions of the Creative Commons Attribution 4.0 International (CC BY 4.0 license) (http://creativecommons.org/licenses/by/4.0/).